Manuscript submitted to: Journal of Geophysical Research - Earth Surface

Celestial Mechanics and Estimating

the Termination of the Holocene

J.A. Parmentola[1]

[1]**The RAND Corporation**

1776 Main Street

Santa Monica, CA 90401

John Parmentola (johnparmentola@gmail.com and jparment@rand.org)

Suggested Reviewers:

Dr. Jacques Laskar

IMCCE, Observatoire de Paris

77 avenue Denfert-Rochereau

75014 Paris

Email : jacques.laskar@obspm.fr

Dr. Chris Poulsen

University of Michigan

Earth and Environmental Sciences

Room 3026
1100 North University

Ann Arbor, MI 48109
phone:(734) 615-2236

Email:poulsen@umich.edu

Dr. S.J. Vavrus

University of Wisconsin-Madison

Center for Climatic Research

1105 AOSS Building

1225 W. Dayton St.

Madison, WI 53706

Phone:(608) 265-5279

Email:sjvavrus@wisc.edu

Key Points:

- A hypothesis is made concerning the percentage change between successive insolation extrema at 65N latitude during June that is testable against climate data.
- A deconvolution model is presented that estimates the precession index and obliquity contributions to these insolation changes.
- The model predictions are shown to correlate with prominent features in the paleoclimate data and enable a low-resolution estimate of the Holocene termination.

Abstract

This paper addresses several issues concerning Milankovitch Theory and its relationship to paleoclimate data over the last 800,000 years. A model is presented that deconvolutes the precession index (precession modulated by the eccentricity) and the obliquity contributions to the percentage change between successive mean-daily-insolation minima and maxima. The sum of these contributions is in close agreement with the corresponding benchmark calculation of J. Laskar et al. The model predictions indicate that the precession index contribution dominates such insolation changes, and its time-dependent behavior correlates with the occurrence of interglacial and glacial periods and temperature trends during these periods. Best fit curves to the separate contributions appear as quasiperiodic waves that correlate with interglacial initiations and terminations through their constructive and destructive interference. However, a comparison of model predictions with the EPICA Dome C (EDC) data indicates delayed inceptions for Marine Isotope Stages 18d and 13c, which have also been noted by Parrenin et al. through a comparison of LR04 benthic δ^{18}O and EDC ice core datasets. Finally, the model enables the classification of interglacial periods into two distinct types that approximately account for their durations. This classification also enables a low-resolution estimation of the Holocene termination based solely on celestial mechanical forcing.

Plain Language Summary

This paper provides new insights into the cause of ice age occurrences over the last 800,000 years based on the earth's celestial motions. The new findings demonstrate that these motions produce recurring trends of amplification and reduction of the sun's rays over the earth's surface that correlate with prominent temperature changes associated with ice ages, the timimg of these occurrences, and the duration of warm periods in the earth's climate history. These results are used to estimate the future termination of the current warm period known as the Holocene.

1. Introduction

Since Milutin Milankovitch's seminal paper[1] concerning the occurrence of ice ages, numerous papers have supported[2-8] and challenged[9,10] his hypothesis that changes in insolation at northern latitudes during the summer solstice is the

likely cause of ice sheet changes associated with ice age occurrences. A substantial number of papers have connected eccentricity, precession, and obliquity cyclical behaviors to features in the paleoclimate data[10,112]. For example, these celestial parameters, as well as the insolation, exhibit specific characteristic frequencies that are also found in spectral analyses of paleoclimate data over the Pleistocene[13]. However, this approach does not completely account for interglacial and glacial durations and the timing of the prominent temperature excursions in paleoclimate data, such as those exhibited in EDC ice core data[14].

In his original papers[1], Milankovitch proposed that the obliquity played a dominant role in ice age occurrences because it affects the insolation at northern latitudes where ice and snow can accumulate on the earth's comparatively large landmass. However, this hypothesis is still unproven, and the quantitative roles of the eccentricity and precession in the earth's paleoclimate history remain an active area of research[12]. Consequently, the eccentricity, precession, and obliquity contributions to the insolation and their correlation with paleoclimate data remain uncertain.

Finally, the behaviors of these three celestial parameters have been used to identify past interglacial periods like the Holocene[15-17]. This form of pattern recognition has enabled quantitative estimates of the Holocene termination. However, such estimates would be much more convincing if the conditions of the Holocene termination due to celestial mechanical forcing coincided with all other past interglacial terminations.

The new results presented here clarify these issues. The provisional assumption is that the percentage change between successive mean-daily-insolation maxima and minima (insolation half-cycles) significantly influenced the timing and duration of prominent features in paleoclimate data, such as the major temperature excursions in the EDC ice core data[14]. This assumption has the added advantage that the precession index and obliquity contributions to the percentage change between successive mean-daily-insolation maxima and minima can be deconvoluted quantitatively. This separation enables insight into their cyclical behaviors and amplifying, and dampening effects on the insolation over extended periods. As it turns out, both contributions are quasiperiodic, which is a consequence of the aperiodic nature of the earth's eccentricity, precession, and obliquity. However, their cyclical behaviors differ from these celestial parameters. This cyclical complexity and their individual insolation behaviors approximately correlate with prominent EDC ice core data features.

Section II briefly describes the basic assumption and emphasizes the quasiperiodic eccentricity, precession, and obliquity behaviors. Section III presents a deconvolution model along with its predictions for the obliquity and precession index contributions to the percentage change between successive mean-daily-insolation extrema. The sum of these contributions is compared with the corresponding theoretical calculations of J. Laskar et al.[18,19]. Comparisons are also made between the cyclical behaviors of the three celestial parameters and those of the precession index and obliquity contributions to the percentage change

between successive insolation extrema. In Section IV, the model predictions are compared with the EDC dataset. Timing discrepancies between the EDC data and the model are identified; however, evidence is presented that suggests the model predictions could be correct. In Section V, a low-resolution estimate for the Holocene termination is presented. A possible physical mechanism within the earth's climate system is also proposed to account for the significant declines in temperature associated with ice ages; however, this proposal is a conjecture requiring further research. In Section VI, the agreement between the data and the model, as well as timing discrepancies and their suggested resolution, are summarized.

2. Background

The sun's solar irradiance is a persistent effect on the earth's atmosphere distributed over its surface (the insolation) through its shape and quasiperiodic celestial mechanical motions. These motions cause the insolation at a latitude to oscillate in an aperiodic manner about an average value. Its magnitude varies depending on the earth's distance from the sun, the direction the earth's axis points, and its tilt angle.

The main point of this paper is to provide insight into the insolation's time-dependent behavior through its separation into precession index and obliquity contributions. This separation reveals that the precession index contribution amplifies and reduces the insolation while the obliquity is a much smaller and narrowly bound contribution to the insolation. Both quasiperiodic behaviors are shown to correlate with the prominent features in paleoclimate data over the last 800,000 years.

This paper assumes the percentage change between successive mean-daily-insolation maxima and minima at 65 degrees northern (65N) latitude during the summer solstice (June) over the last 800,000 years, substantially influenced the prominent features in paleoclimate data such as the EDC dataset depicted in Figure 1,

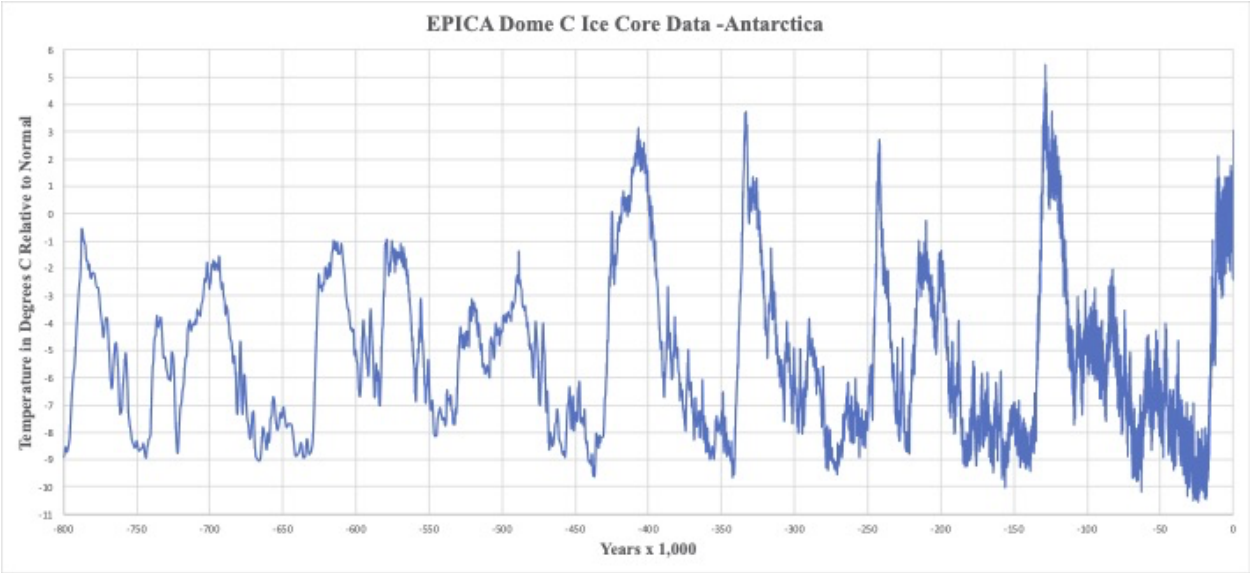

Figure 1. EDC ice core data based on a temperature reconstruction model using deuterium as a proxy presented in degrees centigrade relative to normal from -800,000 years to the present, https://www.ncei.noaa.gov/access/paleo-search/study/6080**.**

Figure 1 is a temperature reconstruction from ice core data using deuterium as a proxy; however, it's model-dependent. Physical effects can affect the dating of temperature changes inferred from ice cores. As discussed in Section IV, such effects become evident when deconvolution model predictions are compared to the EDC ice core data.

Over the last 800,000 years, the mean-daily-insolation at 65N latitude during June underwent 74 transitions between successive maxima and minima, as indicated in Figure 2,

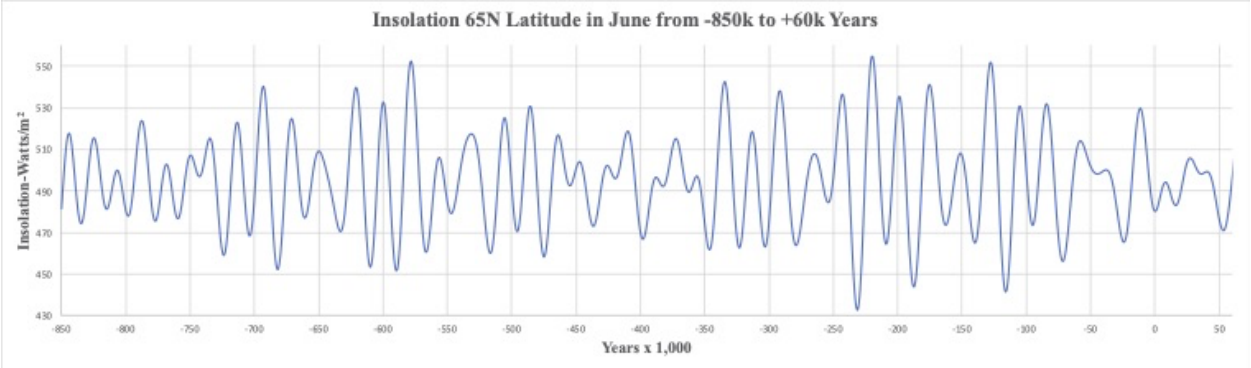

Figure 2. Mean-daily-insolation at 65N latitude in June for the period -850,000

to +60,000 years from J. Laskar, calculated using the IMCCE Virtual Observatory Solar System Portal, CNRS Observatory, Paris http://vo.imcce.fr/insola/earth/online/earth/online/index.php.

These transitions range in percentage from about 28% to -19% (in some cases exceeding 100 Watts/m^2 in magnitude) with half-cycle durations (the average is about 11,000 years) that range from 4,200 to 16,900 years.

Reconciling the 74 transitions of Figure 2 in terms of timing and amplitude with the prominent temperature excursions in Figure 1 is a formidable theoretical challenge. These features are affected by eccentricity, precession, and obliquity cyclical behaviors, which have been computed from -250 million to +250 million years[18,19]. According to the Milankovitch hypothesis, their determination provides a consistent temporal calibration that should correlate insolation changes with features in the paleoclimate data.

There has been considerable discussion in the literature concerning the cyclical durations of the eccentricity, precession, and obliquity and their correlation with various paleoclimate proxy data[11-13]. However, these durations correspond to frequencies of spectral power density maxima, which can obfuscate their complex individual aperiodic behaviors. These complex cyclical behaviors affect the percentage change between successive insolation maxima and minima that is represented in Figure 3,

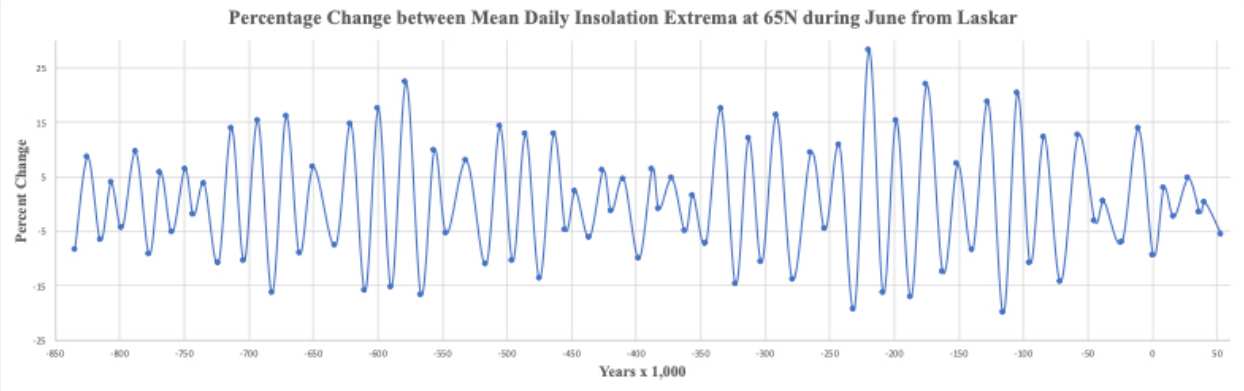

Figure 3. Percentage change between successive mean-daily-insolation maxima and minima at 65N latitude in June during -844,200 to +53,5,000 years from J. Laskar, calculated using the IMCCE Virtual Observatory Solar System Portal, CNRS Observatory, Paris http://vo.imcce.fr/insola/earth/online/earth/online/index.php.

Note, the blue curve in Figure 3 is the best fit to a sparse set of points from -844,200 years to +53,500 years that should not be trusted for numerical precision between these points. However, the timing accuracy of extrema percentage changes and the qualitative behaviors between these points will be utilized to interpret paleoclimate data.

As will be demonstrated, the complex "beat structure" in Figure 3 is a result of the superposition of recurring precession index wave packets (formed from a precession "carrier wave" that is amplitude modulated by the eccentricity) and obliquity wave contributions to the percentage change between successive mean-daily-insolation extrema. However, the half-cycle durations of the precession carrier and obliquity wave contributions are shown in Section III to be significantly different from the half-cycle durations of the three celestial parameters. Nevertheless, the recurring precession index wave packets will be shown to correlate with temperature trends in the EDC dataset and the recurrence of interglacial and glacial periods in Section IV. It is also shown that the obliquity wave contribution correlates with the temperature excursions in the paleoclimate data; however, there are timing differences between the obliquity wave and the temperature excursions. These timing differences are ameliorated through the constructive and destructive interference of the recurring precession index wave packets with the obliquity wave.

3. The Deconvolution Model

This section separates the fractional change between successive mean-daily-insolation maxima and minima into precession index and obliquity contributions. This separation is accomplished, in part, through an application of the computational tool developed by J. Laskar, http://vo.imcce.fr/insola/earth/online/earth/online/index.php, The sum of these estimated contributions will be compared to Laskar's prediction. In what follows, the eccentricity, precession, obliquity, and insolation parameters are specified with a temporal resolution of 100 years using Laskar's tool.

The insolation, Q, is assumed to be of the form,

$$Q = A \bullet B \tag{1}$$

, where A and B are respectively the precession index and obliquity contributions to the insolation. In Appendix A, B is shown to depend on latitude and the sun's declination angle. Because daylight hours depend on latitude and the sun's declination angle, the mean-daily-insolation, $\overline{Q}$, is dependent on the mean-daily-obliquity contribution, $\overline{B}$. By averaging equation (1) over daylight hours, the mean-daily-insolation is given by

$$\overline{Q} = A \bullet \overline{B} \tag{2}$$

It's straightforward to show from equation (2) that the fractional change in $\overline{Q}$ produced through changes in A and $\overline{B}$ is approximately given by

$$\frac{\overline{Q}}{\overline{Q}_i} \cong \frac{A}{A_i} + \frac{\overline{B}}{\overline{B}_i} \tag{3}$$

, where $\frac{A}{A_i}$ and $\frac{\overline{B}}{\overline{B}_i}$ are respectively the fractional precession index and obliquity contributions to the fractional change in the mean-daily-insolation, $\frac{\overline{Q}}{\overline{Q}_i}$, with $\overline{Q} = \overline{Q}_f - \overline{Q}_i$, $A = A_f - A_i$, *and* $\overline{B} = \overline{B}_f - \overline{B}_i$ are the respective changes in the mean-daily-insolation, and the precession index and obliquity contributions to the mean-daily-insolation with the subscripts, i and f, designating the initial and final states. The correction cross-term, $\frac{A}{A_i} \bullet \frac{\overline{B}}{\overline{B}_i}$, to equation (3) will be shown to be negligible.

3.1 Precession Index Contribution

The earth's eccentricity has varied by more than an order of magnitude from about 0.004 to 0.05 during the last 800,000 years. While the eccentricity is cyclical, it's not periodic. In terms of timescales, its average half-cycle duration has been about 47,000 years; however, this duration has varied between about 30,000 to 71,000 years, as indicated in Figure 4,

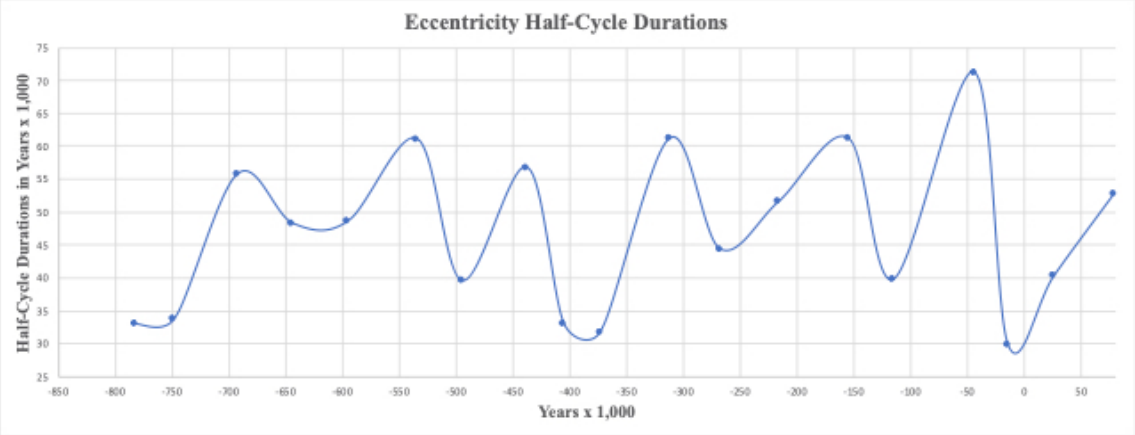

Figure 4. Eccentricity half-cycle durations during the period -815,000 to +79,000 years from J. Laskar,

calculated using the IMCCE Virtual Observatory Solar System Portal, CNRS Observatory, Paris http://vo.imcce.fr/insola/earth/online/earth/online/index .php

The key to understanding the eccentricity's effect on the insolation at northern latitudes during the summer solstice is its change from the time the earth's axis points toward the sun at perihelion to the time it points toward the sun at aphelion. While the timescale of the precession index contribution to the insolation is affected by the eccentricity, its short-term half-cycle is primarily due to the precession. The average precession half-cycle duration has been about 11,000 years; however, precession half-cycle durations have varied between about 7,000 to 15,000 years, as indicated by the following graph,

Figure 5. Precession half-cycle durations during the period -843,900 years to +54,200 years computed from J. Laskar, calculated using the IMCCE Virtual Observatory Solar System Portal, CNRS Observatory, Paris http://vo.imcce.fr/insola/earth/online/earth/online/index.php.

The relatively small eccentricity changes over these precession half-cycles enable the approximate determination of the precession index contribution to the fractional change between mean-daily-insolation extrema. As discussed further below, the precession index contribution to the percentage change between successive insolation extrema at 65N during June takes the form of a quasiperiodic wave; however, its half-cycle durations differ from those of the precession.

Assuming the insolation depends on the inverse distance squared[20] from the sun multiplied by an overall constant, the fractional change of the precession index contribution during a perihelion to aphelion half-cycle transition is given by

$$\frac{A_{p\to a}}{A_p} = \frac{(1-e_p)^2}{(1+e_a)^2} - 1 \tag{4}$$

, where the perihelion subscript, p, and aphelion subscript, a, are the initial and final states, respectively. Equation (4) is well approximated by

$$\frac{A_{a\to p}}{A_a} \approx -2\left(e_a + e_p\right) + e_p^2 + 4e_a e_p + 3e_a^2 \tag{5}$$

, where the linear term dominates. Similarly, in transitioning from aphelion to perihelion, the corresponding fractional precession index contribution is given by

$$\frac{A_{a\to p}}{A_a} = \frac{(1+e_a)^2}{(1-e_p)^2} - 1 \tag{6}$$

, which is also well approximated by

$$\frac{A_{a\to p}}{A_a} \approx 2\left(e_a + e_p\right) + e_a^2 + 4e_a e_p + 3e_p^2 \tag{7}$$

.

, where again the first term dominates, and the subscripts have corresponding interpretations. The eccentricity, e, depends on time and, in what follows, is specified by Laskar's tool at the time of each mean-daily-insolation maximum and minimum during June at 65N latitude.

3.2 Obliquity Contribution

The obliquity involves small angular changes ranging from a minimum of 22.1 to a maximum of 24.5 or 2.4 degrees. Because the obliquity oscillates about an average angle, its contribution to the insolation at a given latitude is also in the form of a quasiperiodic wave. The average obliquity half-cycle duration has been about 20,000 years over the last 850,000 years; however, it has ranged from approximately 18,000 to 23,000 years, as indicated in Figure 6,

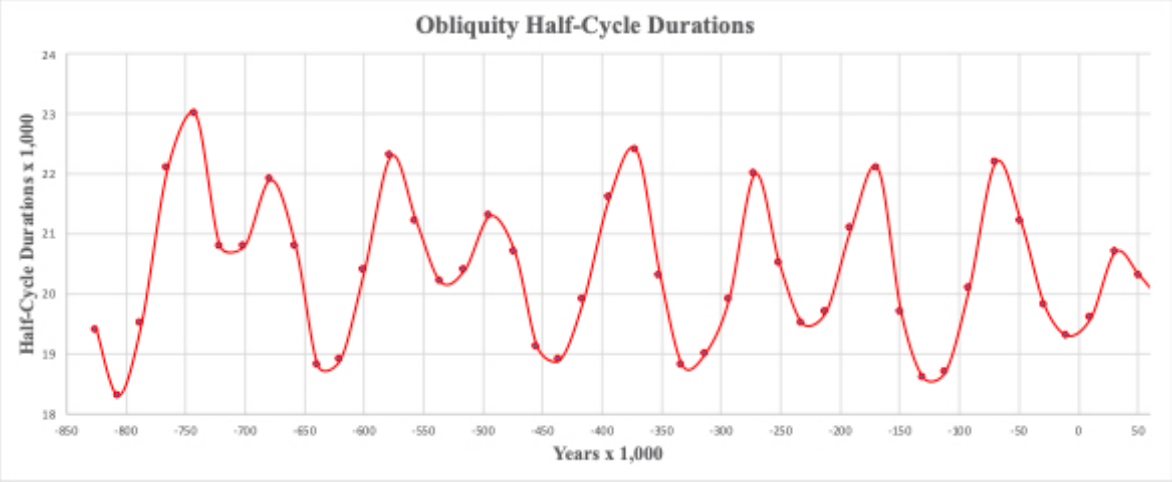

Figure 6. Obliquity half-cycle durations during the period -844,700 years to +51,100 years computed from J. Laskar, calculated using the IMCCE Virtual Observatory Solar System Portal, CNRS Observatory, Paris http://vo.imcce.fr/insola/earth/online/earth/online/index.php.

The comparatively small and gradual change in the earth's tilt angle also enables the approximate determination of the obliquity contribution to the fractional change between successive mean-daily-insolation extrema. As discussed further below, the half-cycle durations of the obliquity contribution to the percentage change between insolation extrema differ from those of the obliquity.

By specializing to the summer solstice (the sun's declination angle equals the obliquity angle), in Appendix A, the fractional obliquity contribution to successive mean daily insolation during June is shown to be of the form,

$$\frac{\overline{B}}{\overline{B}_i} = \frac{h_f \bullet \sin\emptyset \bullet \sin\theta_f + \cos\emptyset \bullet \cos\theta_f \bullet \sin h_f}{h_i \bullet \sin\emptyset \bullet \sin\theta_i + \cos\emptyset \bullet \cos\theta_i \bullet \sin h_i} - 1 \tag{8}$$

, where $\emptyset$ is the latitude $= 1.134$ *radians or* $65N$, and $_i$ and θ_f are the initial and final obliquity angles specified in radians with h_i and h_f the initial and final hour angles determined by,

$$h_j = \cos^{-1}\left(-\tan\emptyset \bullet \tan\theta_j\right) \tag{9}$$

, which is also in radians. The obliquity range, $0.386 \leq \theta \leq 0.428$ radians, implies a maximum percentage obliquity contribution to successive mean-daily-insolation extrema during June at 65N latitude is about 8.6% from equations (8) and (9); however, this maximum is never realized (see further discussion below). In what follows, the obliquity angle, θ, is specified by Laskar's tool at the time of each mean-daily-insolation maximum and minimum at 65N latitude during June. For successive insolation extrema transitions, equations (8) and (9) are surprisingly well approximated by

$$\frac{\overline{B}}{\overline{B}_i} \approx 2\bullet\left(\theta_f - \theta_i\right) \tag{10}$$

The linear terms in equations (5), (7), and (10) can be used to provide reasonable "back of the envelope" estimates for the fractional change between successive mean-daily-insolation extrema at 65N latitude during June. However, in what follows, the more accurate deconvolution model predictions are utilized by substituting equations (4), (6), (8), and (9) into equation (3) to compare the model predictions with the corresponding Laskar predictions of Figure 3. This comparison is shown in Figure 7,

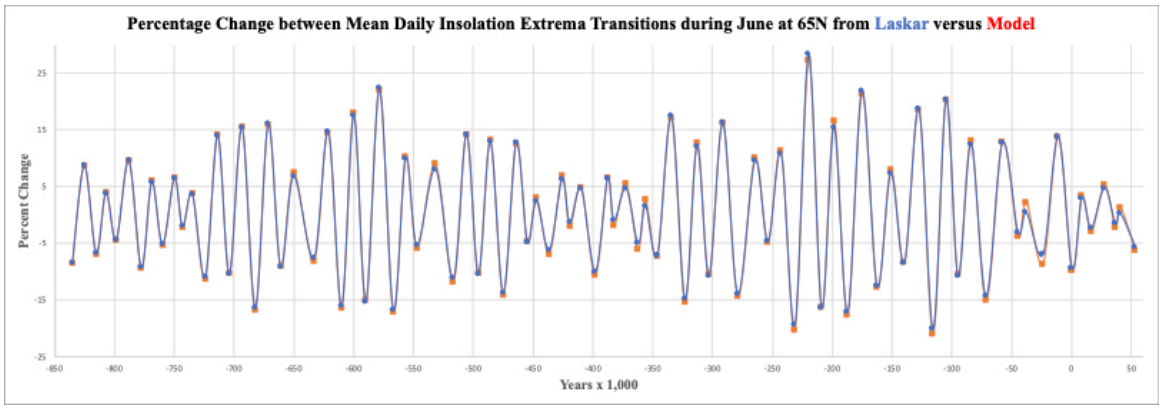

Figure 7. Comparison of the deconvolution model approximation to the percentage change between successive mean-daily-insolation extrema at 65N latitude in June with the predictions of J. Laskar in Figure 3.

In Figure 7, the blue dots follow from Figure 3, and the red dots are deconvolution model estimates for the percentage change between successive mean-daily-insolation extrema at 65N latitude during June. A point wise error analysis of Figure 7 is represented in Figure 8,

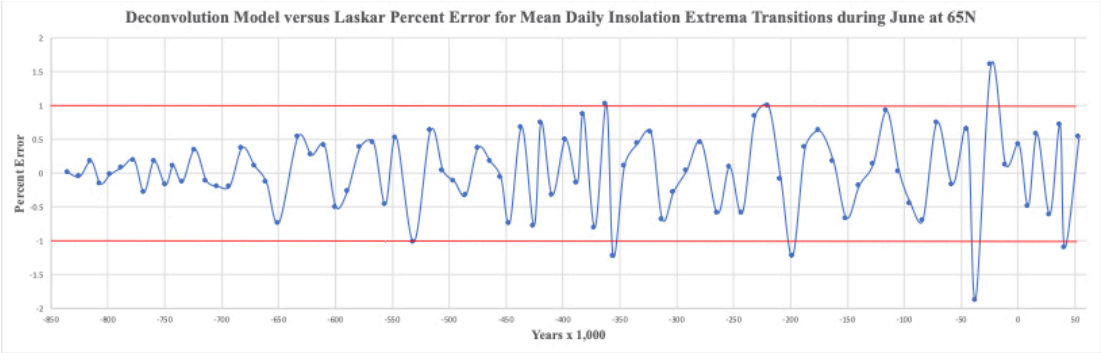

Figure 8. An analysis of Figure 7 indicates a + or -1% error bound on most points (horizontal red lines)

with several points between + or -1 and + or -2%.

For most points, the error is bounded by + or -1%. The comparatively few exceptions are of no consequence to the analysis presented below.

The complex "beat structure" in Figure 7 results from the superposition of the precession index and obliquity contributions to the percentage change between successive mean-daily- insolation extrema, which follow from equations (4), (6), (8), and (9) and are represented in Figure 9,

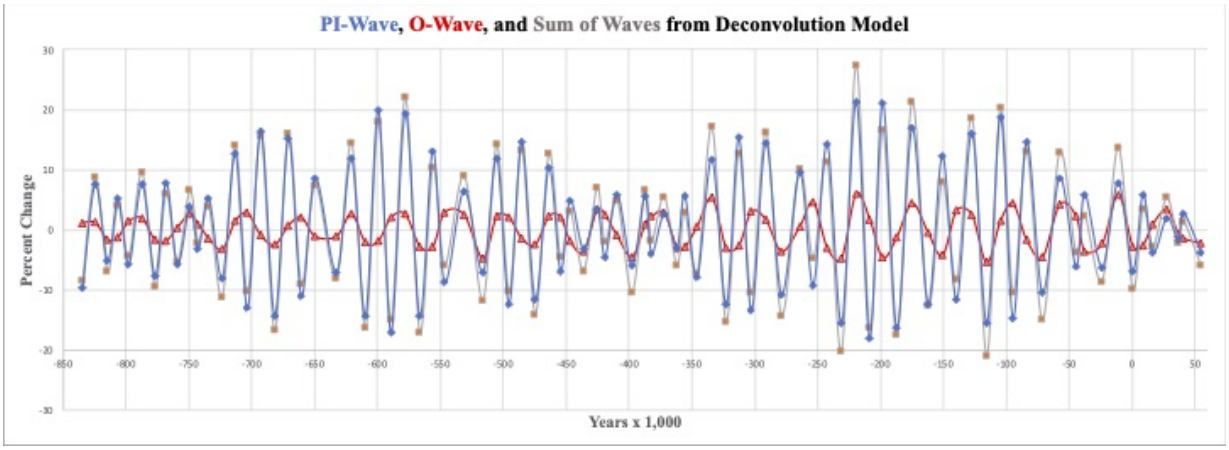

Figure 9. Deconvolution model estimates for the precession index wave (blue curve), obliquity wave (red curve), and their sum (grey curve with red dots) associated with the percentage change between successive mean-daily-insolation maxima and minima at 65N latitude during June from -844,200 to +53,500 years.

The values greater or less than zero represent increasing or decreasing changes from each contribution to successive mean-daily-insolation extrema transitions. They, therefore, provide systematic trends associated with mean daily insolation changes over time, which are not evident in Figure 7. These increasing and decreasing trends will be shown to correlate with the prominent features in paleoclimate data.

Note that the precession index and obliquity contributions to successive mean-daily-insolation extrema from equations (4), (6), (8), and (9) contribute to the neglected cross-term corrections to equation (3). At best, these corrections are an order of magnitude less than the leading terms, which validates equation (3).

The three curves in Figure 9 are based on best fits to a sparse set of points. Therefore, they cannot be trusted for numerical accuracy between the indicated grey, blue, and red points. Nevertheless, the curves provide qualitative features and quantitative estimates as well as a conceptual language involving waves that will be exploited below to physically describe the prominent features of the EDC ice core data of Figure 1.

The obliquity contribution (red curve) in Figure 9 will be referred to as the O-Wave. It appears as an oscillatory wave of varying half-cycle duration having a narrowly bound amplitude. Its contributions range from about 6% (-219,600 years) to -5% (-115,700 years).

The precession index contribution (blue curve) will be referred to as the PI-Wave of recurring wave packets comprised of a precession carrier wave modulated by an eccentricity wave. It's contribution ranges from about 21% (-219,600 years) to -18% (-208,700 years). Note that the eccentricity's primary effect amplifies

and reduces the insolation in a quasiperiodic manner through the recurring PI wave packets.

Finally, the grey curve is the sum of the O-Wave and PI-Wave contributions. Note the O-Wave enhances and diminishes the PI-Wave contribution to the grey curve primarily at its maxima and minima (red dots) in Figure 9. These points and the insolation trends represented by the PI-Wave will play a role in correlating the model predictions with prominent features of the EDC data.

While the magnitudes of the O-Wave maxima are mostly smaller (a factor of four smaller in some cases) than that of the PI-Wave, its half-cycle duration is on average a factor of two greater than that of the precession carrier wave. However, O-Wave half-cycle durations can only be crudely estimated because of the sparse set of points. Nevertheless, the O-Wave varies slowly compared to the precession carrier wave with approximate half-cycle durations that range from about 10,000 to 30,000 years (21,000 years on average), which differ significantly from the obliquity half-cycle durations, as indicated in Figure 10,

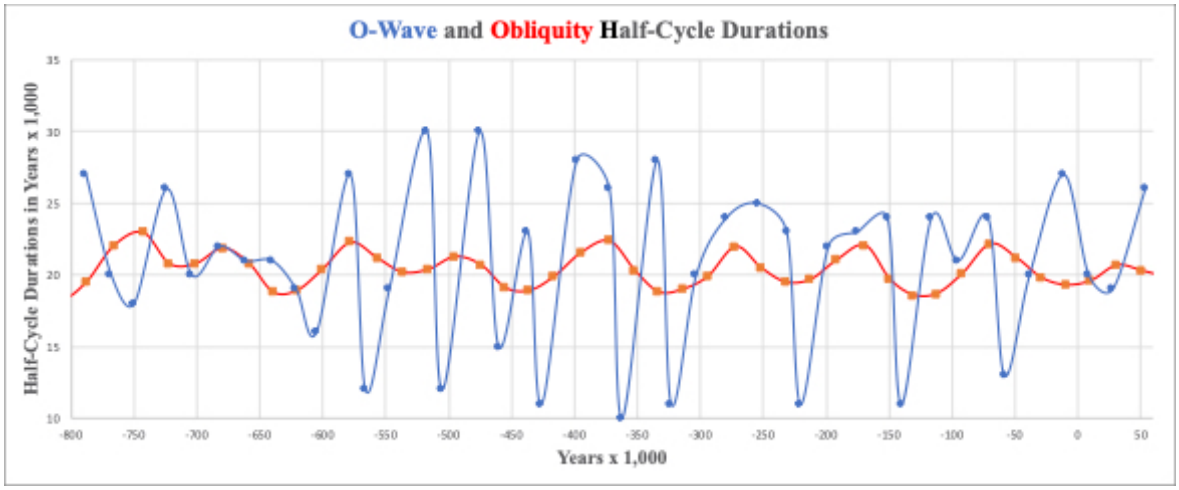

Figure 10. A comparison of O-Wave half-cycle durations inferred from the deconvolution model with obliquity half-cycle durations calculated using the IMCCE Virtual Observatory Solar System Portal, CNRS Observatory, Paris http://vo.imcce.fr/insola/earth/online/earth/online/index.php during the period -787,500 years to +54,000 years.

Note the similar behavior of the O-Wave (blue curve) to the far-left and far-right, which will be discussed further in Section V regarding the Holocene termination.

In Figure 9, the PI-Wave contributions (blue curve) to the mean-daily-insolation extrema transitions are analogous to an AM radio wave having approximate carrier wave half-cycle durations ranging from about 4,000 to 17,000 years (11,000 years on average). In Figure 11, this range (blue curve) differs from the precession half-cycle durations (red curve),

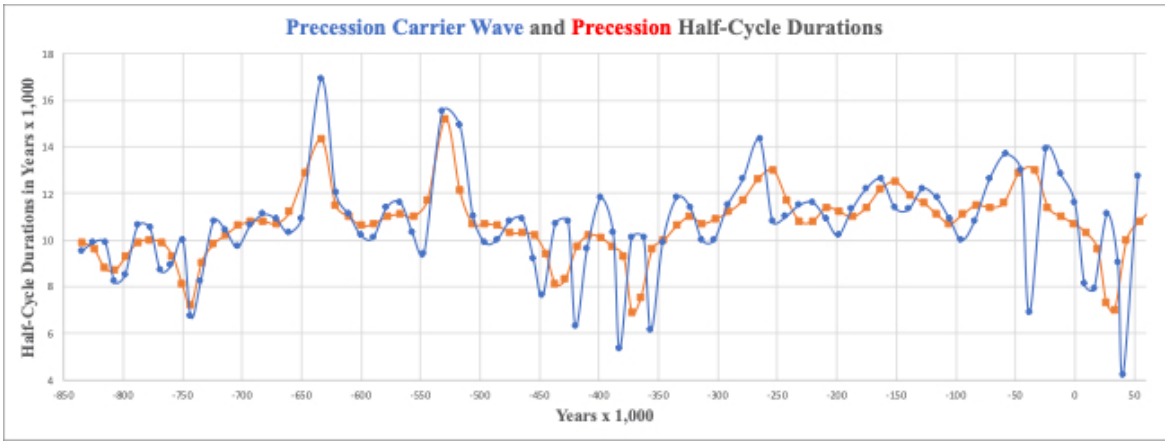

Figure 11. A comparison of precession carrier wave half-cycle durations (blue curve) inferred from the deconvolution model with the precession half-cycle durations (red curve) determined from http://vo.imcce.fr/insola/earth/online/earth/online/index.php during the period -844,200 years to +54,200 years.

Due to the multiple and variable half-cycle durations, a graphical analysis is adopted in the next section to establish correlations between the estimated PI-Wave and O-Wave contributions to successive insolation extrema transitions and the EDC data.

4. Climate History Correlations

Because of the earth's highly complex climate system and unknown conditions in the past, its response to external effects such as celestial mechanical forcing is very challenging to predict. Adding to this complexity are internal effects within the earth system that can also affect its climate, such as volcanic eruptions, albedo changes, etc. Hence, the detailed behavior of the earth's climate between and during interglacial periods is far beyond the scope of this paper. Nevertheless, there are correlations between celestial mechanical forcing and prominent features in the EDC data.

Consider the comparison of Figure 1 EDC data modified by Marine Isotope Stage (MIS) designations[21] with the PI-Wave of Figure 9 represented in Figure 12,

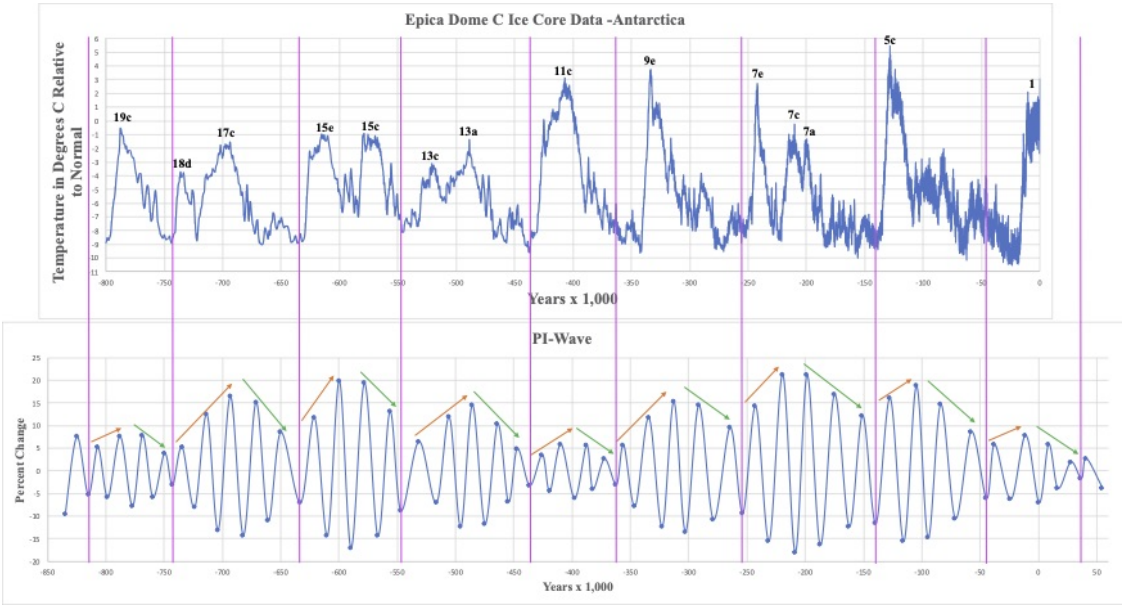

Figure 12. PI recurring wave packets (judiciously defined by purple vertical lines) approximately correlate with interglacial and glacial periods over the last 800,000 years. Precession carrier wave maxima trends approximately correlate with increasing temperature trends (red arrows) and decreasing maxima trends (green arrows) with decreasing temperature.

Visually, the recurring PI wave packets, which are approximately specified by the vertical purple lines, roughly correlate with recurring interglacial and glacial periods. However, the relationship between the timing of prominent temperature excursions and deconvolution model predictions also depends on the O-Wave contributions (see further discussion below). Nevertheless, increasing temperatures in the EDC data coincide with increasing precession carrier wave maxima (red arrows), while declining temperature trends follow the decreasing trend in precession carrier wave maxima (green arrows). These trends in amplitudes are primarily due to eccentricity changes. The eccentricity during precession carrier wave cycles amplifies and reduces the insolation over substantial periods, which roughly correlate with the initiation and termination of interglacial periods.

Note that some temperature trends are interrupted by precession carrier wave amplitude reductions that appear to "split" the temperature peaks into MIS pairs, namely, 18d-17c, 15e-15c, 13c-13a, 7e-7c, and 7c-7a (see further discussion below). Also, note the similarity in Figure 12 between the wave packet to the far left (associated with MIS 19c) and the last one to the far right (associated with MIS 1), which is the Holocene, but more about this relationship later.

The O-Wave contribution to the percentage change of successive mean-daily-insolation extrema also approximately correlates with EDC temperature excur-

sions as indicated in Figure 13,

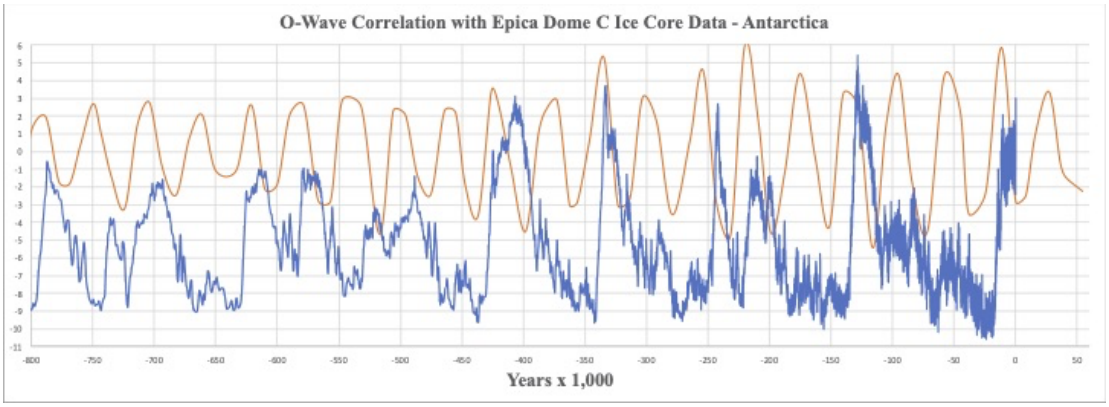

Figure 13. O-Wave predictions from the deconvolution model and EDC data indicate an approximate

temporal correlation between O-Wave maxima and EDC temperature peaks.

Over the last 800,000 years, there were 20 O-Wave maxima (red curve) and 13 prominent temperature excursions (blue curve) with numerous temperature "bumps" in between. Note that from -430,000 years to the present, the obliquity wave maxima tend to be higher, and the minima lower than the period -800,000 to -430,000 years. This behavior may, in part, account for the systematically higher and lower temperatures during the period -430,000 years to present compared to the earlier period.

In Figure 14, the temporal correlation between the O-Wave and EDC temperature excursions can be improved by shifting the EDC data by -10,000 years,

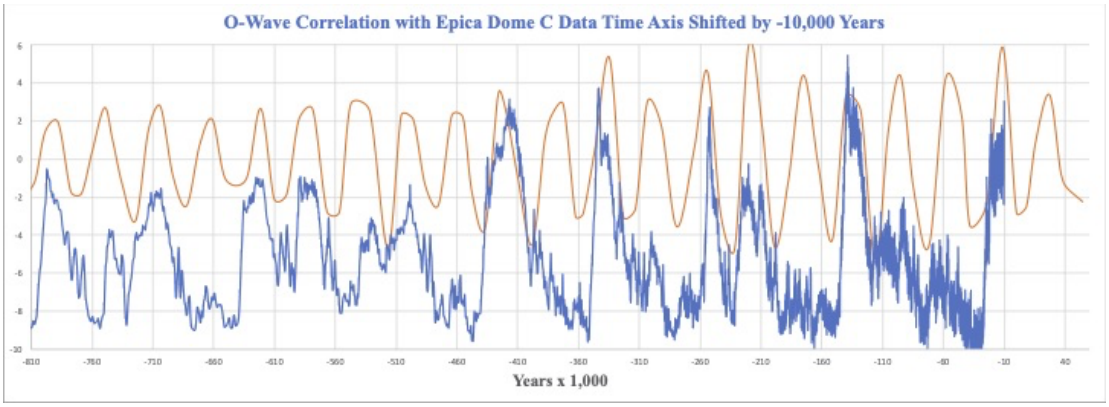

Figure 14. O-Wave predictions from deconvolution model and EDC data temporally shifted by -10,000

years indicating an improved temporal correlation between O-Wave maxima and

EDC temperature peaks.

Note, the 10,000-year shift is comparable to the average precession carrier wave half-cycle duration. In what follows, the timing differences between the O-Wave contribution and the temperature excursions are ameliorated through interference between the PI- and O-Wave.

Utilizing the above wave taxonomy, interglacial periods can be classified into two types. Those of Type I occur over one precession carrier wave cycle. During such a cycle, there is an approximate constructive interference between the precession carrier and O waves. Those of Type II occur over two precession carrier cycles; however, there is constructive and destructive interference between the precession carrier and O waves during such cycles.

Using MIS designations, those of Type I are 19c, 15e, 15a,13c, 9e, 7e, 5e, and 1, which are represented in Figure 15,

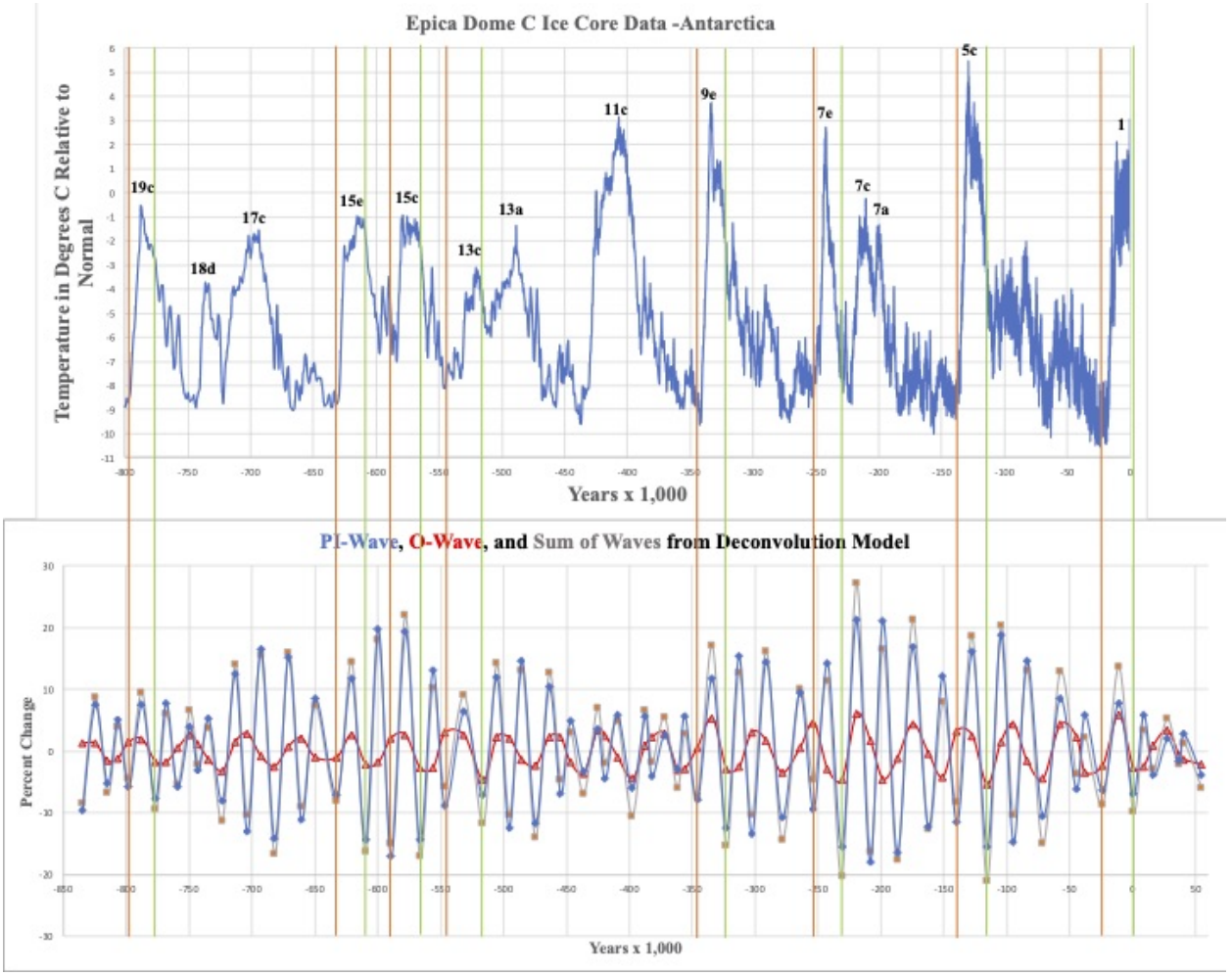

Figure 15. Type I interglacial initiations (red vertical lines) are followed by interglacial terminations (green vertical lines). Initiations coincide with concurrent PI-Wave, and O-Wave increases to the right of the red vertical lines, and terminations coincide with corresponding concurrent declines ending in green vertical lines.

Each pair of vertical red and green lines extending across both graphs relates the duration of each precession carrier cycle and its corresponding MIS interglacial. For Type I, all PI-Wave contributions constructively interfere with O-Wave contributions except for MIS 7e (see further discussion below). Starting from the right of each vertical red line, both contributions concurrently increase to approximately synchronized maxima associated with the red dots of the grey curve and then decline concurrently to the vertical green lines terminating on the red dots of gray curve minima. The vertical green lines define all interglacial

terminations, which are comparatively sharp. Note the role of the O-Wave is to enhance (constructive interference) the precession carrier wave maxima and minima as indicated by the red dots associated with grey curve maxima (excluding for MIS 7e) and minima (including MIS 7e). The termination of MIS 1, the Holocene, will be discussed in the next section.

For MIS 7e, the PI- and O-Wave contributions are initially out of phase by about ¼ of an O-Wave cycle; however, they partially constructively interfere as the PI-Wave contribution increases to the right of the indicated vertical red line. The duration of this interglacial is likely cut short because the O-Wave contribution subsequently destructively interferes with the PI-Wave contribution. However, MIS 7e terminates like all others of Type I as indicated by the deep minimum at the green line (the grey curve red dot minimum).

Note also, the delay in the initiation of interglacial MIS 13e, which has the longest precession carrier wave cyclical duration of about 30,000 years. Its precession carrier wave maximum represents a decline from the earlier maximum in Figure 15. Also, the amplification rate of the insolation during this period is comparatively low due to its long duration. This delay is described further below, along with another initiation delay associated with a Type II interglacial.

The interglacial periods of Type II are MIS 18d, 17c, 13a, 11c, and 7c-7a. The latter hyphenated designation is further explained below. Each of these periods involves a pair of precession carrier wave maxima trending higher, as depicted in Figure 16,

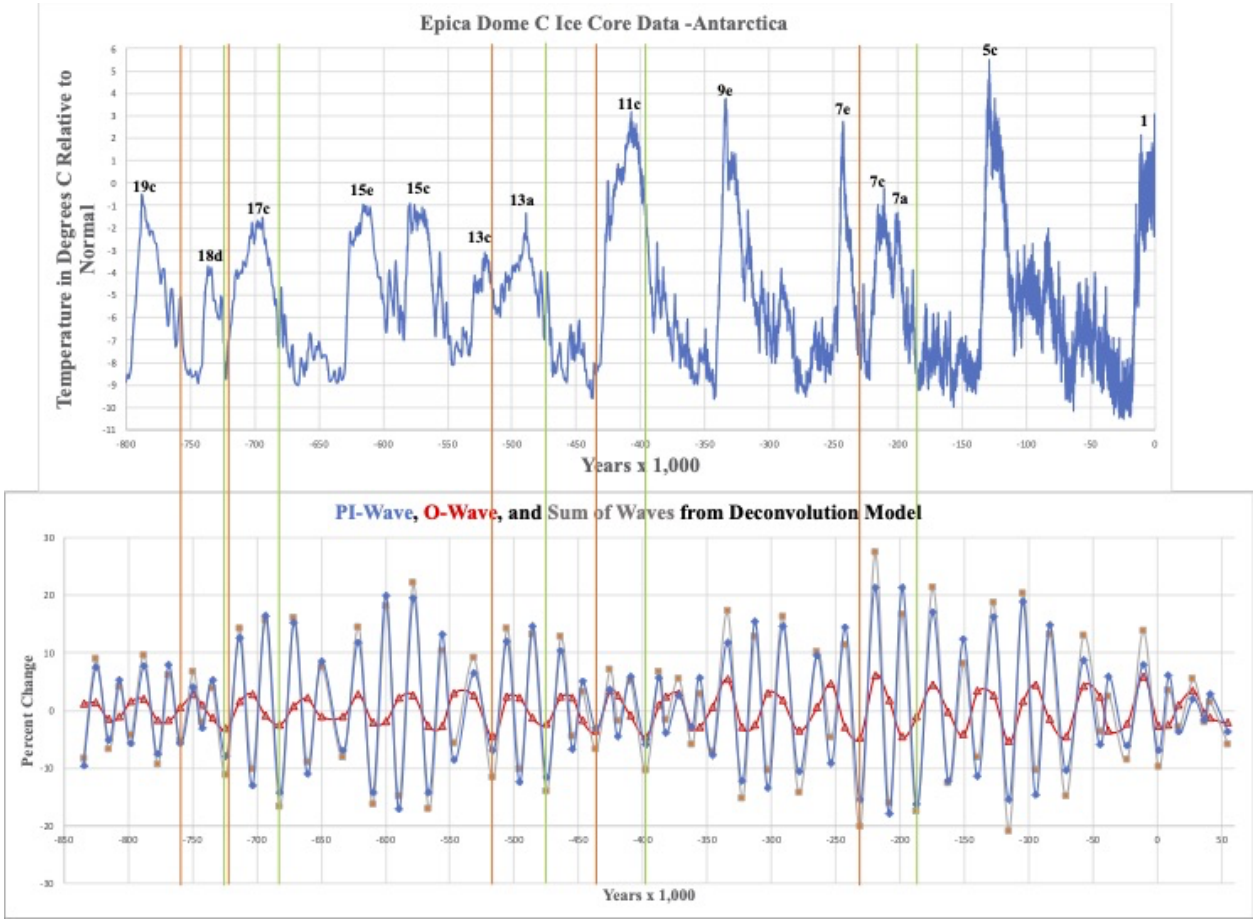

Figure 16. Type II interglacial initiations (red vertical lines) are followed by interglacial terminations (green vertical lines). Initiations coincide with concurrent PI-Wave and O-Wave increases to the right of the red vertical lines, while terminations coincide with corresponding declines ending in green vertical lines. Note that the pair of green and red lines associated with the MIS 18d-17c split the interglacial.

Again, the pair of vertical red and green lines identify the temporal extent of two precession carrier wave maxima and minima and their corresponding interglacial period. The O-Wave contributions occur over a longer half-cycle than the Type I set. In all cases, an O-Wave maximum is approximately in phase with the first precession carrier wave maximum (constructive interference). The O-Wave is then out of phase with the next precession carrier wave minimum and maximum (destructive interference). Eventually, the O-Wave contribution ends approximately in phase with the final precession carrier wave minimum except for MIS 7c-7a, which is about ¼ of an obliquity wave cycle out of phase (about 11,000 years). However, in the latter case, the O-Wave contribution is

negative at the second precession carrier wave minimum, so it constructively contributes to the MIS 7a termination as indicated by the deep minimum at its green vertical line (red dot minimum of the grey curve).

MIS 7c-7a appears to be an interglacial that is split in two. It is associated with successive precession carrier wave maxima and minima that have the largest magnitudes over the last 800,000 years. There is a concurrent decline in the precession carrier wave and O-Wave contributions between the precession carrier wave peaks. The timing of this concurrent decline likely accounts for the split in the MIS 7c-7a interglacial. However, the MIS 7a temperature peak is of a very short duration, likely due to the destructive interference between the second precession carrier wave peak and the O-Wave. Note that MIS pairs 18d-17c, 15e-15c, 13c-13a, and 7e-7c also appear to be split by PI- and O-Wave cyclical behaviors.

All Type I and II interglacial durations are approximately determined by their precession carrier wave durations. However, there are delays in the initiation of MIS 18d (5,000–7,000 years) and MIS 11c (11,000–13,000 years). For MIS 18d, the precession carrier wave maximum to the right of the red line is a part of an insolation decline despite its enhancement from the O-Wave contribution (red dot on grey curve). The subsequent second precession carrier wave maximum (MIS 18d is of Type II) is even less by about 2%. This feature may account for the comparatively small MIS 18d temperature excursion. The relatively low rate of increasing insolation may also account for the comparatively small MIS 11c temperature excursion.

Both MIS 18d and 11c also represent deep ice cores (time is a function of core depth), where physical effects can affect the estimated time of these interglacial inceptions and terminations using ice core models. It has been noted by Parrenin et al.[22] that the most significant timing discrepancies between paleoclimate datasets EDC and LR04 benthic δ^{18}O occur for MIS 18d and 13c. This comparison suggests that the deconvolution model predictions for the timing of interglacial initiations and terminations could be correct.

Overall, the rates of insolation amplification as indicated by the recurring PI wave packets (enhanced by the obliquity contribution) appear to correlate with rising EDC temperature excursions. Similarly, the rates of insolation decline represented by the recurring PI wave packets (reduced by the O-Wave contribution) correlate with persistent temperature declines. All interglacial terminations coincide with the same celestial mechanical forcing conditions.

5. Estimating the Holocene Termination

The analysis presented above indicates that MIS 1 is a Type I interglacial. As such, it is expected to terminate because of PI- and O-Wave constructive interference. The MIS 1 one cycle classification indicates that MIS 11c is an unlikely analog, which has been proposed in the literature by A. Berger et al.[15].

MIS 19c has also been identified as a possible Holocene analog based solely

on the behavior of celestial parameters and comparable mean-daily-insolation changes[15]. The analysis presented below addresses the similarities and differences between MIS 19c and MIS 1 based on PI- and O-Wave contributions to the percentage change between successive mean-daily-insolation extrema at 65N latitude during June.

As pointed out earlier in Figure 10, the O-Wave half-cycle durations of MIS 19c and MIS 1 are similar. They both are associated with an O-Wave cycle duration of about 37,000 years, with approximate half-cycles of 27,000 years on the upside and 10,000 years on the downside. They also have comparable declines in mean-daily-insolation from their maxima to minima. For MIS 19c, the decline is about 48 Watts/$m^{2,}$ while for MIS 1, it's about 50 Watts/m^2.

Their main difference is the estimated duration of their precession carrier wave cycle and half-cycle durations. For MIS 19c, the precession carrier wave cycle duration is about 21,000 years, while for MIS 1, it's about 24,000 years. This difference indicates that MIS 1 will likely be a longer interglacial than MIS 19c. In terms of interglacial terminations, the MIS 19c downside precession carrier wave half-cycle duration is about 10,500 years, while for MIS 1, it is about 11,600 years.

In Figures 15 and 16, Type I and II terminations end on grey curve red dot minima that involve O-Wave enhancements (constructive interference) to precession carrier wave minima. The following Table 1 summarizes the termination estimates for each MIS based on their downside precession carrier wave half-cycle duration,

Type I	MIS #	Termination (years)
	19c	10,500
	15e	11,100
	15a	11,700
	13c	14,800
	9c	11,400
	7e	11,500
	5e	11,800
	1	11,600
Type II	18d	10,800
	17c	11,100
	13a	10,800
	11c	11,800
	7c-7a	11,200

Table 1. MIS termination duration estimates

based on the last precession carrier wave peak to

the vertical green line in Figures 15 and 16.

These termination estimates are all comparable (within hundreds of years of each other) in duration except for MIS 13c, which has the longest cyclical duration and the largest downside precession carrier wave half-cycle duration of 14,800 years.

Assuming the vertical green line for MIS 1 in Figure 15 is accurate, its termination will occur within about 500 years from the present; however, exactly when cannot be determined just from celestial mechanical forcing. This estimate coincides with the local minimum in insolation using Laskar's tool as indicated in Figure 17,

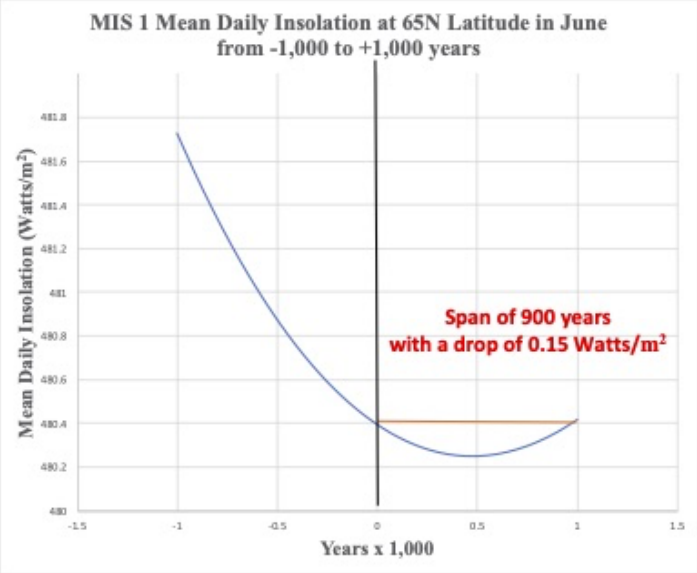

Figure 17. MIS 1 mean-daily- insolation at 65N latitude during June from -1,000 to +1,000 years. The shallow minimum at +500 years measured from the vertical black line estimates the Holocene termination, which coincides with the vertical green line in Figure 15.

This estimate is of low resolution because the above minimum is very shallow. The earth will remain in this shallow minimum for at least 900 years. MIS 19c shares the same feature as indicated in Figure 18,

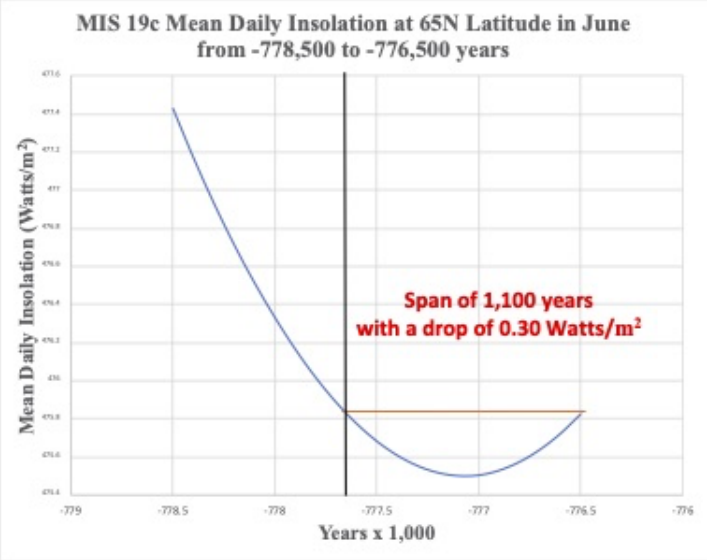

Figure 18. MIS 19c mean-daily-insolation at 65N latitude during June from -778,500 to -776,500 years. The shallow minimum at 600 years measured from the vertical black line is a termination estimate that coincides with the vertical green line in Figure 15.

, which also has a relatively shallow minimum over 1,100 years. Note that all other interglacial terminations share this common feature.

Given the consistent recurrence of the interglacial terminations based on celestial mechanical forcing over the last 800,000 years, it is likely that there is a common physical mechanism that accounts for interglacial terminations. Milankovitch Theory focuses on northern latitudes at or greater than 65N because of the potential for ice sheet growth due to the decline in mean-daily-insolation at these latitudes during June over thousands of years. The substantial reduction in the mean-daily-insolation over 11,100 years for the Holocene has likely had a cooling effect on the air over a range of latitudes. This latitudinal range is due to a tradeoff between increasing insolation as the latitude decreases (the obliquity has decreased over the last 11,100 years) along with a concurrent decline in daylight hours. As examples, Figures 19 and 20 demonstrate the extensive nature of this latitudinal effect for MIS 19c and 1,

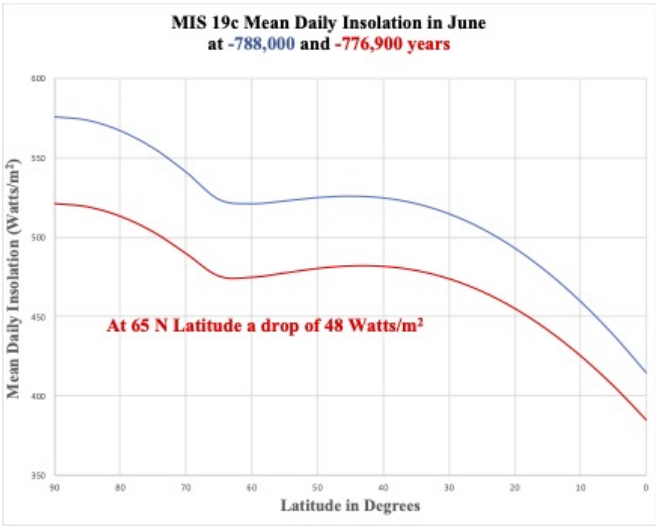

Figure 19. Latitudinal effect on mean-daily-insolation over a period of 11,100 years for MIS 19c.

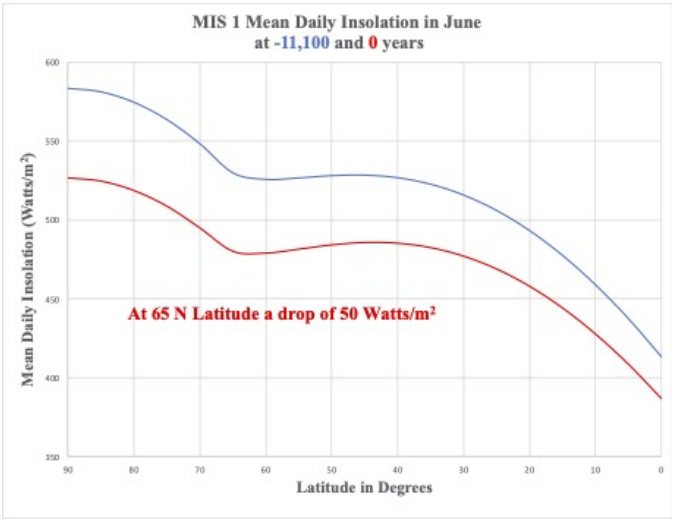

Figure 20. Latitudinal effect on mean-daily-insolation over a period of 11,100 years for MIS 1.

This gradual reduction in mean-daily-insolation over the last 11,100 years enables air at northern latitudes to more readily cool during the winter solstice (the hour angle significantly decreases), which has the potential to increase the dense cold air volume at northern latitudes. In recent times, the cold air volume above 60N latitude has resulted in extreme weather events associated with an instability of the polar vortex - stable cold, dense air counter-rotating at northern

latitudes - that is kept in check by the jet stream. The specific conditions that produce these events are not well understood due to the lack of a reliable theory of the earth's climate. At best, there are models[23] that attribute different physical mechanisms to these events. However, the recurrence of such events over an extended period can result in ice and snow accumulation that can change the earth's albedo, producing cooler climates because of gradual changes in the earth's heat engine.

It's essential to keep in mind that the above estimated MIS 1 termination is tentative. Nevertheless, based solely on celestial mechanical forcing, the Holocene termination is likely to happen as all other interglacial terminations over the last 800,000 years.

6. Conclusions

The deconvolution model presented here provides additional insight into the roles of the precession index and obliquity contributions to the insolation. In particular, the recurrence of interglacial and glacial periods over the last 800,000 years approximately correlates with the quasiperiodic of PI wave packets. This correlation is reinforced by the quasiperiodic behavior of the O-Wave contribution to the insolation. In addition, all interglacial inceptions and terminations involve constructive interference between the PI and O waves. Finally, interglacial durations roughly coincide with the number and duration of precession carrier wave cycles. These new results support Milankovitch Theory.

However, the comparison between the model predictions and EDC data indicates two timing inconsistencies. There are delays in interglacial inceptions associated with MIS 18d and 13c; however, these may be due to physical effects related to deep ice cores. Nevertheless, the roles of the PI and O waves predicted by the deconvolution model should motivate further examination of paleoclimate data tuning. In this regard, further progress on improving estimates of O-Wave cyclical durations would likely enhance the time calibration of the observed features in paleoclimate data.

Finally, given the recurrent PI- and O-Wave pattern associated with interglacial terminations, the search for a common physical mechanism related to the earth's future climate becomes more compelling. It is likely that a cumulative effect occurs over an extended period (the next 500 years) that eventually tips the earth into a persistent temperature descent concurrent with the decline in precession carrier wave maxima. This trend very likely impairs recovery until there is a return to increasing precession carrier wave maxima as Figure 12 indicates. Identifying the specific physical mechanism that causes this descent is far beyond the scope of this paper. Nevertheless, the potential expansion of the cold air volume at northern latitudes due to significant declines in insolation over the last 11,100 years should be investigated as a possible cause. Given recurring PI wave packets and their correlation with interglacial and glacial periods over the last 800,000 years, the catastrophic consequences to the future of civilization from another ice age should provide ample motivation to intensify scientific

research in this vitally important area for all of humanity.

Acknowledgments

I would like to acknowledge numerous exchanges with Professor William H. Smith of Washington University, St. Louis, concerning Milankovitch Theory. I would especially like to thank Dr. Patrick Frank of the Stanford Linear Accelerator Center for reading the manuscript and making numerous helpful suggestions that measurably improved the clarity and presentation of the results. I am also indebted to Bruce Bauer, Data Manager, World Data Service for Paleoclimatology and NOAA National Centers for Environmental Information (NCEI) Climatic Science and Services Division – Paleoclimatology Boulder, CO for providing the relevant paleoclimate datasets. Finally, I would like to express my gratitude to Dr. Jacques Laskar for directing me to the wonderful computational tool he and his colleagues created, which enabled all the computations in this paper.

Appendix A

This section aims to derive equations (8) and (9) using light rays and vector analysis. The sun's light rays hit the earth with uniform intensity at angles relative to tangential planes over the earth's surface. However, there is a point on the earth where the rays are perpendicular to a tangential plane, the subsolar point. As the earth rotates, this point moves westward and north and south due to the earth's obliquity and orbit in a wavelike pattern completing an entire cycle over a year.

For an observer at a point on the earth looking vertically, there is a component of a solar ray parallel to the vertical and another tangential. The vertical component is of interest in determining the obliquity contribution to the insolation, while the tangential component is assumed lost. The key quantity to determine is the time-dependent zenith angle between an observer vector pointing vertically and the declination vector pointing from the earth's center to the subsolar point. The deconvolution model assumes that the cosine of this angle times an overall constant determines the obliquity contribution to the insolation. Because the observer and subsolar point move relative to the sun, the mean daily insolation is the average of the cosine of the zenith angle over daylight hours.

The relevant angles and vectors defined with respect to the earth's body fixed rotating axes are represented in the following diagram,

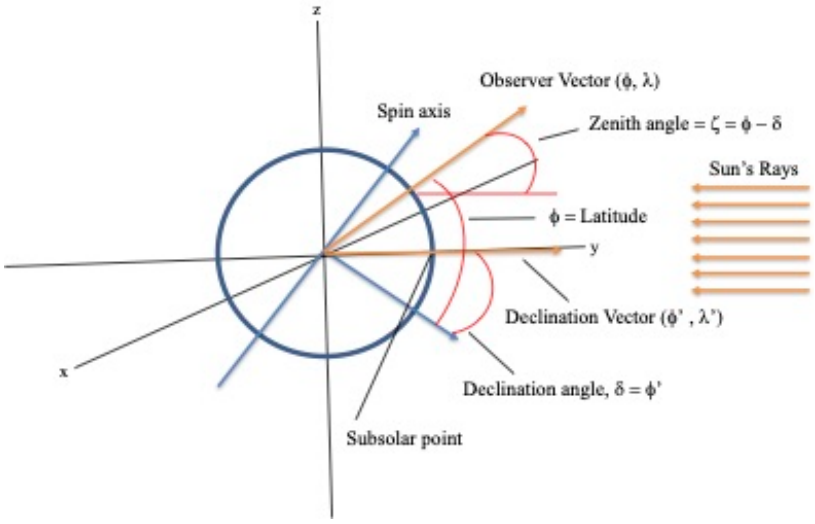

Figure 1A. A diagram that defines the relevant vectors of the observer and declination in terms of their latitudes and longitudes, (f , l) and (f'= d, l'), respectively defined with respect to rotating body fixed axes. The observer latitude and the declination angle, d, determine the zenith angle, z.

The observer unit vector in the rotating body-fixed frame is given by,

$$\vec{V_o} = \ cos(\emptyset) \bullet cos(\lambda)\, \vec{i} + sin(\phi) \bullet cos(\lambda)\, \vec{j} + sin(\lambda)\, \vec{k} \qquad (1A)$$

, and the declination unit vector is given by,

$$\vec{V_\delta} = \ cos(\emptyset') \bullet cos\left(\lambda'\right)\, \vec{i} + sin\left(\phi'\right) \bullet cos\left(\lambda'\right)\, \vec{j} + sin\left(\lambda'\right)\, \vec{k} \qquad (2A)$$

, where $\emptyset' = \ \delta$, the declination angle. The cosine of the zenith angle is simply the scalar product of equations (1A) and (2A) given by,

$$\vec{V_o} \bullet \vec{V_\delta} = cos(\zeta) = sin(\phi) \bullet sin(\delta) + cos\ (\phi) \bullet cos(\delta) \bullet cos(h) \qquad (3A)$$

, where $h = \lambda' - \ \lambda$ is the hour angle, which for sunrise and sunset is determined by $\cos(\zeta) = 0$ or

$$h_0 = \ \cos^{-1}\left(-\tan(\emptyset) \bullet \tan(\delta)\right) \qquad (4A)$$

, which equals equation (9) for the summer solstice when $\delta = \ \theta$, the earth's obliquity angle.

For the deconvolution model, we assume the obliquity contribution to the insolation during the summer solstice is of the form

$$B = G\bullet(\ \sin(\phi) \bullet sin(\theta) + cos\ (\phi) \bullet cos(\theta) \bullet cos(h)) \tag{5A}$$

, where G is an overall constant. The mean daily obliquity contribution to the mean daily insolation, $\overline{Q}$, of equation (2) is obtained by averaging equation (5A) over daylight hours given by

$$\overline{B} = \frac{G}{2 \bullet \pi} \bullet \int_{-h_0}^{h_0} (\ sin(\phi) \bullet sin(\theta) + cos(\phi) \bullet cos(\theta) \bullet cos(h))\, dh \tag{6A}$$

$$= \frac{G}{\pi} \bullet (h_0 \bullet\ sin(\phi) \bullet sin(\theta) + \cos(\phi) \bullet cos(\theta) \bullet sin\,(h_0)) \tag{7A}$$

, from which equation (8) follows straightforwardly with h_0 determined by equation (4A) with $\delta = \theta$.

References

1. Milankovitch, M., "Theorie mathematique des phenomenes thermiques produits par la radiation solaire", Gauthiers-Villars, Paris; Royal Serb. Acad., Spec. Publ., 133, pp. 1-633 (1941).

2. Hays, J.D.; Imbrie, John; Shackleton, N.J. 1976, Science. 194 (4270): 1121–32.

3. Imbrie, J. 1982, Icarus, Vol. 50, Issues 2-3, pp. 408-422.

4. Imbrie, J., & Imbrie, K. P. 1986, Ice Ages: Solving the Mystery (MA: Harvard University Press).

5. J. Zachos, M. Pagani, L. Sloan, E. Thomas, and K. Billups, 2001, Science, Vol. 292, Issue 5517, pp. 686-693.

6. Gradstein, F., Ogg, J., & Smith, A. 2005, A Geologic Time Scale 2004 (Cambridge University Press).

7. Huybers, P. 2011, Nature, Vol. 480, pp. 229–232 and references therein.

8. Roe, G., 2006, Geophysical Research Letters, Vol. 33, L24703, doi:10.1029/2006GL027817 and references therein.

9. Wunsch, C., 2004, Quaternary Science Reviews, Vol. 23, Issues 9-10, pp, 1001-1012.

10. Berger, W.H., 2012, Scripps Institution of Oceanography Technical Report, Milankovitch Theory - Hits and Misses, https://escholarship.org/uc/item/95m6h5b9, and references therein.

11. Lisiecki, LE. and Raymo, M.E., 2005, Paleoceanography, Vol. 20, PA1003, pp.1-17 and references therein.

12. Lisiecki, L., Nature Geoscience, Vol. 3, pp. 349–352.

13. Meyers S.R., Sageman B.B., and Pagani M., American Journal of Science, June 2008, 308 (6), pp. 770-786.

14. The EDC dataset is available at https://www.ncei.noaa.gov/access/paleo-search/study/6080. For a history of ice core science see, Jouzel, J., Climate of the Past, Vol. 9, pp. 2525-2547.

15. Vavrus, S.J., He, F., Kutzbach, J.E. et al., Scientific Reports, Vol. 8, Article number: 10213.

16. Berger, A., Loutre, M.F. and Crucifix M., Surveys in Geophysics, Vol. 24, pp. 117–138.

17. Rohling, E.J., Braun, K., Grant, K., Kucera, M., Roberts, A.P., Siddall, M, Trommer, G., Earth and Planetary Science Letters 291 (2010) 97–105.

18. All computations in this paper make considerable use of the computational tool by J. Laskar et al., http://vo.imcce.fr/insola/earth/online/earth/online/index.php.

19. For a summary of the history of celestial mechanical computations relevant to insolation quantities of the earth, see Laskar, J., Robutel, P., Joutel, F., Gastineau, M., Correia, A.C.M., and Levrard, B., Astronomy and Astrophysics, Vol. 428, pp. 261-285 and references therein.

20. In deriving equations (4) and (6), the earth-sun distances at perihelion, $R_p = a \bullet (1 - e_p)$, and aphelion, $R_a = a \bullet (1 + e_a)$, are used, where, a, is the semi-major axis of the earth's orbit. The semi-major axis is assumed constant during an insolation transition between successive extrema, which implies eccentricity changes result from changes in the semi-minor axis. Also, because the eccentricity is a slowly varying function of time, differences in the time specification of insolation extrema and when the earth's axis successively points toward the sun at perihelion and aphelion and vice versa have a comparatively small impact on the insolation. This assessment is consistent with the comparison of deconvolution model results for the percentage change between successive insolation extrema at 65N during June and those of J. Laskar et al as represented in Figure 7 and the error analysis in Figure 8.

21. See Reviews of Geophysics, March 2016, Review Article, 10.1002/2015RG000482, pp. 1-58.

22. Parrenin, F. et al., Climate of the Past, 3, pp. 485-497, 2007, Figure 3, pp. 7.

23. See Geophysical Review Letters, December 2021, https://agupubs.onlinelibrary2 Materials and Methods